Scalable electrohydrodynamic drying configuration for dehydrating biological materials at industrial scale

Kamran Iranshahi[1,2], Daniel I. Onwude[1], Donato Rubinetti[1], Alex Martynenko[3], Thijs Defraeye [1,2] *

[1]Empa, Swiss Federal Laboratories for Materials Science and Technology, Lerchenfeldstrasse 5, CH-9014 St. Gallen, Switzerland

[2] ETH-Zurich, Swiss Federal Institute of Technology, Zurich 8092, Switzerland

[3]Dalhousie University, Faculty of Agriculture, Truro, Nova Scotia, Canada

Abstract

Electrohydrodynamic drying (EHDD) is an energy-efficient and novel method for non-thermal dehydration of plant-based foods, especially fruits and vegetables. Upscaling EHD drying to dry biological materials like fruits and vegetables at an industrial scale is a current challenge of this technology, which hinders the implementation in industry. This paper experimentally evaluates the scalability of an optimized electrode configuration for EHD dryers. Unlike conventional EHDD studies, in which the collector electrode is a metallic plate, we employ a new design with a mesh with few conductive wires as a collector. This design was selected based on an in-silico optimization study aiming to improve energy efficiency. The performance of this novel emitter-collector configuration is characterized and compared with the conventional EHDD setup. Drying kinetics and energy consumption in different fruit loading densities are quantified as performance indicators to evaluate the scalability of different EHDD configurations. In addition, the overall performance of all EHDD configurations is compared with a commercial hot-air dryer from energy consumption and drying kinetics perspectives. Our experiments show that the new EHDD design leads to more uniform dehydration than the conventional EHDD configurations employed in previous studies. In addition, it significantly improves the specific drying rate by more than 65% and energy consumption by more than 60% for loading densities higher than 0.5 kg m-3. Compared to the commercial hot-air dryer, the novel EHDD configuration is 2.6 times more energy efficient. However, the drying rates of the EHDD configurations are lower than the commercial hot-air dryer. These significant improvements of the EHD dryer with the optimized and up-scalable mesh collector could provide the push needed to finally implement EHDD as an industrial unit in full-scale.

Keywords: Food processing; Industrial dryers; Ionic wind; Postharvest; Corona discharge; EHD

* *Corresponding author: thijs.defraeye@empa.ch (T.Defraeye) Empa, Swiss Federal Laboratories for Materials Science and Technology, Laboratory for Biomimetic Membranes and Textiles, Lerchenfeldstrasse 5, CH-9014 St. Gallen, Switzerland*

1. INTRODUCTION

The increasing global population demands more effective actions regarding food security. One of these actions could be reducing food waste which plays a pivotal role in the food supply chain. Currently, 30% of the produced food is wasted worldwide [1,2]. Preserving food by drying is a traditional yet effective method to reduce food waste by facilitating the storage and transportation of food. Examples of foods that are dried include fruits and vegetables, meat, fish, milk powder, and herbs. Moreover, dried fruits are desirable as healthy snacks for consumers and currently account for a significant portion of consumers' diet [3]. However, drying is an energy-intensive and time-consuming process due to the latent heat of evaporation that is needed to remove water [4]. Being energy-intensive is a challenge towards implementing drying facilities, especially in low-income countries with limited energy resources. Therefore, researchers are actively seeking to develop energy-efficient and sustainable drying methods. In this regard, electrohydrodynamic drying (EHDD) is a promising non-thermal drying technique with a high potential to be used as a sustainable drying method [5]. A high voltage power supply and emitter and collector electrodes are the main components of an EHD drying device. The air around the emitter will be ionized when a high voltage is applied between the electrodes. The movement of these ions from the emitter towards the collector induces an airflow with speeds ranging from 0.1 to 10 m s^{-1}, depending on the applied electric power. The EHD generated airflow contains ions and is called ionic wind. The ionic wind provokes convective dehydration on drying materials. This drying technique has gained the attention of researchers in the last decades due to its promising features, such as low energy consumption, non-thermal processing, and superior quality of the final product [6,7].

Previous studies evaluated EHDD from different aspects such as drying kinetics, energy consumption, and dried food quality [8,9]. In the previous EHDD experiments, usually, a plate is used as a collector in a horizontal drying chamber (e.g., [10–12]). However, the scalability of these designs to an industrial level is not satisfactory [13]. Scalability is defined as the ability of a system to adjust its production capacity through system reconfiguration with minimal cost in a minimal time [14,15]. The two main principles of scalability are replication (i.e., scale-out) and upgrade (i.e., scale-up) [15]. Replication in an industrial system refers to the capability of the system for an unrestricted increase or decrease of the production capacity, or so-called loading density, without deteriorating its performance. Upgrade refers to the system's ability to keep its functionality during dimensional scaling, i.e., increase or decrease in size.

Despite being the most studied configuration, the conventional plate collector is not scalable as it does not meet the replication and upgrade requirements. Regarding the replication, the modeling study of Defraeye and Martynenko [13] showed that the performance of the plate collector, in terms of fast and uniform drying, deteriorates by increasing the amount of the loaded drying material. Moreover, upgrade in plate collector is limited too. The airflow cannot pass through the plate, so an EHD dryer with the plate collector cannot be scaled to have multiple rows of drying trays with the same drying performance due to the aerodynamics considerations [16]. Therefore, scalability is one of the hurdles in the industrialization of this technology.

Recently, our numerical investigations showed that employing a mesh as a collector leads to a more uniform drying and could significantly improve the performance of the EHDD in terms of energy consumption and drying rate [16]. Mesh screens (or perforated plates) have been widely used in standard convective dryers (e.g., [17,18]). Numerical investigations predicted that mesh collectors could significantly improve the drying rate [5]. To improve the energy efficiency, our numerical study showed that the mesh should be made of non-conductive wires and a few conductive wires in certain locations that are grounded or connected to a negative high voltage [16]. Nevertheless, the performance of these promising designs has only been proven numerically and they are not tested experimentally.

In this study, we introduce an optimized and scalable experimental setup that has the potential to be used as a pilot plant. The performance of this novel configuration is analyzed by quantifying drying kinetics and energy consumption via several performance indicators such as specific energy consumption, drying rate, and critical drying time. To evaluate the upscaling potential, the performance of this novel design is evaluated for various fruit loading densities. All these performance indicators are compared with the previous studies on EHDD to determine the added values of this scalable experimental setup.

2. MATERIALS AND METHODS

2.1. Experiments

2.1.1. Sample preparation

The Pink Lady apples were purchased from a local grocery store in St. Gallen, Switzerland. The initial wet basis (wb) moisture contents of the sample ranged between 85± 0.2% to 87± 0.6% [g g_{wb}^{-1}] which is equivalent to 5.71±0.1 to 6.8±0.1 [g g_{db}^{-1}] in dry basis (db). The apples were peeled and rinsed with water. The surface water of samples was removed using a towel. The slices were cut longitudinally from the main axis of the fruit using an electric food slicer (Domo DO1950S, LINEA 2000, Belgium) in different thicknesses. The thickness of the slices varied between 2 to 5 mm for different experiments. Slices were further cut to 30 mm × 30 mm squares for the experiments with a cutter. This shape simplified calculations of evaporation area and loading density. The sliced apple samples were put into the dryer immediately after cutting to reduce surface enzymatic browning. The moisture content of the dried apple slices was measured by dehydrating the samples in a drying oven (105 ± 1 ℃) until a constant weight according to the approved method of the Association of Official Analytical Chemists (AOAC)[19].

2.1.2. Experimental setup

a) EHD experimental setup

An optimized upscalable EHD drying setup was designed based on the multiphysics-based simulation results [16] and previous experiments ([20]). A schematic diagram of the experimental setup is shown in Figure 1a. The main components are a lab-scale convective chamber (40×40×70 cm), discharge (emitter) and collecting electrodes, a digital scale (PG5001-S, Mettler-Toledo, Greifensee, Switzerland, 0.1 g resolution to record the weight of the samples on the computer every 60 seconds), and a direct current (DC) high voltage power supply of positive and negative polarity (Spellman_SL30PN10 0～30kV). The emitter and collector electrodes were connected to the positive and negative high voltage power supplies, respectively. The samples were placed on the collector. In order to avoid any disturbance in the airflow distribution close to the samples by the digital scale, a suspended weighing system was used. This non-intrusive approach allowed us to measure the sample's weight loss in real-time. The surface temperature of the slices was monitored every 5 minutes using an IR camera (Flir A40, FLIR Systems Inc., Wilsonville, USA). The relative humidity (RH) and ambient temperature at the inlet and outlet of the test box were monitored during the experiments using the Sensirion SHT31 sensors (Sensirion, Stäfa, Switzerland). The discharge energy consumption was measured by reading the current and voltage between electrodes using a multimeter (Keysight U1253B, Santa Rosa, CA, USA) and a 1000:1 high voltage probe (Testec HVP-40, Testec Elektronik GmbH, Germany). The total energy consumption was measured using the MegaPower™ Plug Power Meter (Digiparts, Canada). The flow rate was measured using two hot-wire digital anemometers (Testo 405i, Testo SE & Co., USA). These anemometers were placed in the center of the drying chamber, 20cm above and 40 cm below the collecting electrode close to the inlet and outlet of the drying chamber, respectively. A customized test box (1 m ×1 m × 2 m) was built to control the test condition and respect the safety guidelines regarding working in the high voltage environment (i.e., Faraday cage). The EHD drying chamber and all associated equipment were placed in the test box. All the experiments were carried out inside this box.

b) Discharge and collecting electrodes

Two different emitter-collector configurations were used in this study, namely wire-to-mesh and wire-to-plate configurations. Wire emitters were selected to provide a uniform discharge covering the drying area. In addition, fewer design parameters are involved in up-scaling wires compared to a collection of needles. For instance, needle wire-body radius, tip radius, tip angle, needle body height, and needle arrangement should be optimized when needled are used as emitter [21]. A plate and an optimized mesh were used as collectors (Figure 1b). The optimized wire-to-mesh configuration was selected based on a previous optimization study [16]. The discharge and collecting electrode area was 300 mm ×300 mm = 0.09 m^2. The mesh collector has an 85% open area that consists of conductive and non-conductive wires. The conductive wires (Copper rounded silver-plated wires, Kabletronik, Germany) with a diameter of 0.5 mm were placed in specific locations based on the simulation optimization results (Figure 1b). In this regard, for each emitter wire, four collecting electrodes were located parallel to the emitter wire in horizontal distances of 2.2 cm and 3.4 cm from the emitter wire. The gap (vertical distance) between the collector and emitter was fixed at 5±0.2 cm. This special arrangement of the emitter-collector wires is optimized, replicable, and upgradeable in X, Y, and Z-directions, to respect scalability requirements [15]. Another set of experiments was carried out by replacing the mesh with a solid plate collector (wire-to-plate) to compare our novel design with conventional EHD drying designs used in most previous research on EHDD. The plate was made of an aluminum sheet 2 mm thick with a surface area of 300 mm x 300 mm = 0.09 m^2. A plastic (PVC) holder for the collecting electrode was designed using FreeCAD V0.19 software and milled to house the electrodes properly. The holder was able to accommodate the mesh with different porosities and different locations of the conductive wires.

c) Hot-air drying experimental setup

A hot-air dryer (Rommelsbacher DA 900, Dinkelsbühl, Germany) was used to compare with EHDD. The hot-air drying test was performed at the maximum possible drying temperature (70 ℃) to have the best energy efficiency, as reported in previous studies on hot-air dryers [22]. The surface area and porosity of the hot-air dryer's tray were similar to the mesh collector in wire-to-mesh configuration (0.09 m^2 and 85%, respectively).

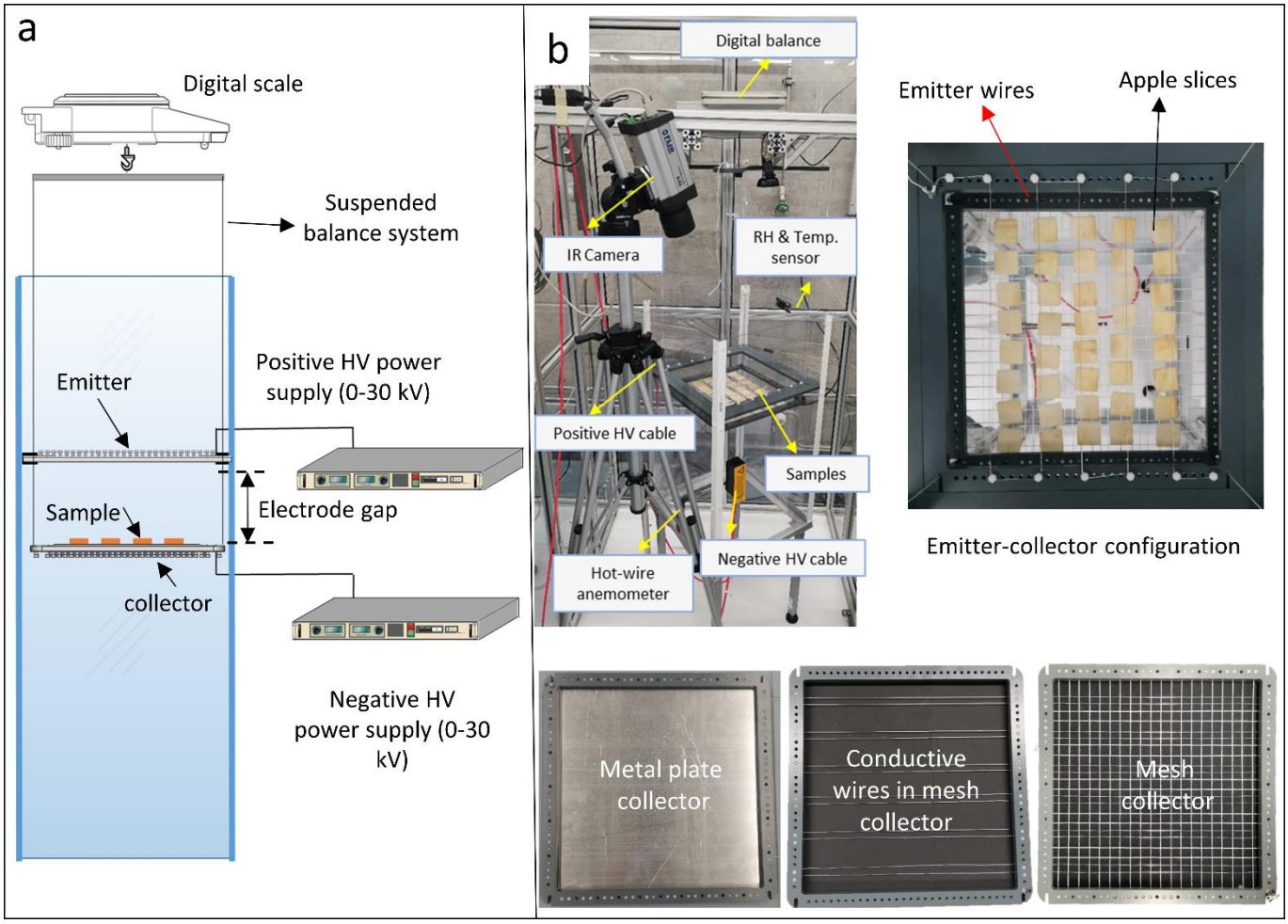

Figure 1a) Schematic illustration of the experimental setup, b) Experimental setup together with the electrodes configuration and plate vs. mesh collectors

2.1.3. Drying experiments

Prior to the experiments, the apples were kept under ambient temperature for 2 hours. Different amounts of fresh-cut square slices have been placed on either a plate or mesh collecting electrodes. Drying experiments were carried out at ambient air conditions (21±0.5 ℃ air temperature and 53±3 % relative humidity). The digital balance measures three forces when the high voltage is applied to the electrodes. These forces include the weight of the samples, drag force due to the airflow blockage by samples and collector, and the electrostatic attraction force between the emitter and collector due to the suspended collector system. Because of the shrinkage of the slices during drying, the covered surface of the collector varies that in turn, affects the drag force. The samples were weighted in both continuous and intermediate modes. In intermediate mode, we turned off the system every 30 minutes to cancel out the electrostatic and drag force effects and measure the weight solely. The continuous mode data (with drag and electrostatics effect) were corrected by the intermediate weighting data.

a) Variable loading density tests

This set of experiments was conducted to evaluate the first principle of scalability, namely replication, by changing the production capacity of the wire-to-plate and the optimized wire-to-mesh configurations. The drying capacity or so-called fruit loading density (LD) varied from 0.4 to 1.2 kg of fruit per m^{-2} of mesh or plate. The collector surface coverage ratio (SCR) varied from 20% to 60%. The drying processes were continued until the product attained the equilibrium moisture content (moisture ratio variation<0.05). The discharge power for loading density tests was set at 12.7±0.1 W by applying +20±1 kV DC voltage on the emitter, -20±1 kV DC voltage on the collector and, 325±5 μA current between emitter and collector. Applying these parameters provided an average electric field strength of 7.8±0.2 kV $cm^{-1,}$ which generated ionic wind with an average velocity of 0.85±0.06 m s^{-1} (at 40 cm below the collecting electrode) and a volume flow rate of 470±30 m^3 h^{-1} for clean tests (no drying material). The selected operating parameters are summarized in Table 1. The motivation for these choices was to keep consistency with our previous experiments and simulations. The same ambient conditions of the wire-to-mesh configuration tests were applied to the wire-to-plate configuration tests.

b) Performance characterization tests of the optimized wire-to-mesh configuration

This set of experiments was conducted to characterize the performance of the novel optimized wire-to-mesh configuration using different discharge powers. To this end, the total discharge power of both negative and positive power supplies was varied from 0

to 11±0.1 W by changing the applied voltage and current according to Table 1. An equal positive and negative DC voltages were applied to the emitter and the collector, respectively. A constant fruit loading density of 0.8 [$kg_{drying\ matter}\ m^{-2}$] was chosen for the characterization tests. Control experiments (natural convection) have been carried out in the same EHD drying chamber without an electric field under the same environmental conditions of the characterization tests.

Table 1 Selected operating parameters for drying tests

Test name	Configuration	Loading density [$kg_{drying\ matter}\ m^{-2}$]	Power [W]	Voltage [kV]	Average current [µA]
Plate LD 0.4	wire-to-plate	0.4	12.7±0.1	40	315±5
Plate LD 0.8	wire-to-plate	0.8	12.7±0.1	40	315±5
Plate LD 1.2	wire-to-plate	1.2	12.7±0.1	40	315±5
Mesh LD 0.4	wire-to-mesh	0.4	12.7±0.1	40	315±5
Mesh LD 0.8	wire-to-mesh	0.8	12.7±0.1	40	315±5
Mesh LD 1.2	wire-to-mesh	1.2	12.7±0.1	40	315±5
Mesh Control	wire-to-mesh	0.8	0	0	0
Characterization 1	wire-to-mesh	0.8	1±0.1	26	40±1
Characterization 2	wire-to-mesh	0.8	5±0.1	29	172±3
Characterization 3	wire-to-mesh	0.8	9±0.1	32	282±3
Characterization 4	wire-to-mesh	0.8	11.2±0.1	32	350±5

2.1.4. Statistical analysis of the data

Measurements were carried out with three replications, and results were expressed as mean ± standard deviation. Changes in drying rate and energy consumption were analyzed using a one-way analysis of variance (ANOVA). The independence of the error terms was verified through randomization. The analysis was completed using R [23]. Statistical difference was determined using the least significant difference (LSD) comparison test (*t*-test) and accepted at p-value < 0.05.

2.1.5. Infrared thermography of drying materials

The surface temperature of the drying materials can effectively be used to monitor the drying process. To this end, thermal images were recorded by a thermographic camera (FLIR A40, Flir Systems Inc., Wilsonville, Oregon, USA) with an infrared resolution of 320 × 240 pixels, a spatial resolution of 1.3 mrad thermal sensitivity below 0.08 °C, and accuracy of ±2 °C operating in the window 7.5–13 µm of the far IR range of the electromagnetic spectrum. The IR camera was placed 1m above the drying chamber to collect data every five minutes during the experiment. The camera was calibrated using a black body (BX-500 IR Infrared Calibrator, CEM, Shenzhen, China). Anti-reflective paper panels were placed at drying chamber walls to minimize the impact of the infrared radiation reflected from the walls. The reflected temperature of the other surfaces was measured according to the standard method described in ISO 18434-1:2008 [24]. The emissivity coefficient of the other surfaces was not significantly different compared to the drying material surface under measurement (p>0.05). In each test, ten samples were randomly selected and the average surface temperature of those samples was used in our analysis.

2.2. Performance indicators

In this section, the indicators for analyzing the performance of different EHD drying configurations are discussed. These indicators are described in two major groups: drying kinetics and energy consumption.

2.2.1. Drying kinetics indicators

a) Moisture content

Variation of the dry basis moisture content and moisture ratio (MR) with time were considered for evaluation of the drying kinetics. The moisture ratio of drying samples at any time was calculated according to the following equation:

$$MR = \frac{MC_{db,t} - MC_{db,e}}{MC_{db,0} - MC_{db,e}} \quad (1)$$

Where $MC_{db,t}$, $MC_{db,e}$and $MC_{db,0}$ are the time-dependent, equilibrium, and initial dry basis moisture contents [$kg_{H2O}\ kg^{-1}{}_{dry\ based}$], respectively.

b) Critical drying time

The critical drying time (t_{crit}) was considered as the reference drying time in all configurations. It is defined as the time needed for the sample to reach the critical moisture content (w_{crit}), which is the averaged moisture content in the sample that corresponds to an equilibrium water activity below which no spoilage occurs [25]. For our experiments on the EHD drying of the apple slices, w_{crit} was considered 37.8 kg $m^{-3,}$ which corresponds to MC_{db} =0.29 [kg_{H2O} $kg^{-1}{}_{dry\ based}$]. Using t_{crit} enables us to have a simple way to compare different drying curves.

c) Drying rate

The average drying rate (DR) in a certain time window [kg_{H2O} h^{-1}] was derived from the moisture loss curve:

$$DR = \frac{evaporated\ water\ mass}{\Delta t} = m_{t2}\frac{MC_{db,t1} - MC_{db,t2}}{t_2 - t_1} \quad (2)$$

Where t_1 and t_2 are the initial and end drying time points [h] of the time range that DR is calculated. $MC_{db,t1}$ and $MC_{db,t2}$ are the dry basis moisture content [kg_{H2O} $kg^{-1}{}_{dry\ based}$] at time t_1 and t_2, respectively. m_{t2} [kg] is the total mass of the samples at t_2. In order to make the drying rate index comparable for different loading densities, a specific drying rate (SDR) was also considered, which is defined as the drying rate per kilogram of drying material [g_{H2O} $kg^{-1}s^{-1}$]:

$$SDR = \frac{DR}{m_0} \quad (3)$$

where m_0 [kg] is the total mass of the fresh-cut drying products loaded on the dryer.

d) Drying flux

Drying flux (DF) in a certain time window was defined as the change in the mass per unit area of samples and per unit time [g m^{-2} s^{-1}]:

$$DF = \frac{DR}{A_s} \quad (4)$$

where A_s [m^2] is the total area of the fresh-cut drying material.

e) Drying capacity

Loading density (LD) [$kg_{drying\ matter}$ $m^{-2}{}_{of\ collector}$] and surface coverage ratio (SCR) [%] are the indicators of the drying capacity. LD is defined as the total mass of the fresh-cut drying matter loaded to the dryer per total tray area, and SCR is the percentage ratio of the total sample area to the collector area.

2.2.2. Energy consumption indices

Energy consumption can be calculated in two ways: total and discharge energy consumption. The total energy consumption refers to overall energy consumed, including high voltage power supply losses and auxiliary tools. This value is highly equipment-dependent and changes with the scale of the equipment. For example, the impact of a relatively inefficient high-voltage supply is higher on a lab-scale setup than an industrial unit, given the size of the drying area. Therefore, the energy use of the corona discharge process, i.e. discharge energy, is preferred as a scale-independent indicator of energy consumption [26]. Discharge energy consumption does not include the high voltage power supply losses and other auxiliary tools. It is basically the energy consumed after the high voltage power supply. In EHDD studies, discharge energy is usually used for comparison purposes.

a) Specific energy consumption (SEC)

Specific energy consumption (SEC) [J $kg_{H_2O}{}^{-1}$] is defined as the net energy E [J] used to evaporate a unit mass of water Δm [kg]. It is a robust index for comparing the energy performance of the drying processes because it includes a quantity reflecting the drying kinetics of a product. It can be calculated by dividing the discharge power P [W] by the average drying rate over the full drying process until the critical drying time is reached:

$$SEC = \frac{P}{DR(t_{crit})} = \frac{V.I.t_{crit}}{m_{eva}} \quad (5)$$

P [W] is the discharge power of the drying process that for EHD drying process it can be calculated by multiplying of voltage V [V] and current I [A]:

$$P = V.I \quad (6)$$

b) Specific moisture extraction rate (SMER)

Specific moisture extraction rate (SMER) [kg_{H_2O} kWh^{-1}] is another performance index, which is used to describe the effectiveness of the energy used in the drying process [27]. It is simply the inverse of the specific energy consumption and is given by the ratio

between the total moisture removed to the total energy input. In theory, the maximum SMER value for a conventional drying unit is 1.55 kg_{H_2O} kWh^{-1}, which is the latent heat of water evaporation at 100 °C [28].

$$SMER = \frac{amount\ of\ water\ evaporated}{E_{in}} \tag{7}$$

c) Energy efficiency of the drying process

The energy performance of a drying process is characterized by various indices. The energy efficiency (η_E) is a frequently reported index for evaluating the energy performance of the dryer [29]. It is defined as the energy used for moisture evaporation at the solids feed temperature (E_{ev}) to the total energy supplied to the dryer (E_{in}) [30];

$$\eta_E = \frac{E_{ev}}{E_{in}} = \frac{(m_{eva})(C_P \Delta T + L_{eva})}{P(t_2 - t_1)} \tag{8}$$

where m_{eva} is the evaporated water mass [kg], C_P is the specific heat capacity of water at constant pressure (≈ 4200 $J{\cdot}kg^{-1}{\cdot}K^{-1}$ at 20 °C), and L_{eva} is the latent heat of evaporation (≈2450 kJ kg^{-1} at 20 °C). In this paper, t_{crit} is considered as the reference drying time thus $t_2 - t_1$ in the above equation can be replaced by t_{crit}.

3. Results

In this section, we compare the experimental result of performance evaluation in the optimized-scalable EHDD setup with the conventional setups.

3.1. Impact of the EHDD configurations on the drying kinetics

3.1.1. Drying time and drying rate

The drying kinetics for the optimized-scalable mesh collector and conventional plate collector are evaluated in this section. The results are shown in Figure 2, Table 2, and Figure 3. Increasing the loading density does not significantly affect the drying kinetics of the optimized wire-to-mesh (Figure 2a and c). On the other hand, the performance of the wire-to-plate configuration in drying kinetics deteriorates by increasing the loading density. The difference between the drying performances in higher loading densities is attributed to the different airflow distribution on the plate and mesh (Figure 3). The wire-to-mesh configuration enables convective dehydration from all the surfaces of the sample. In contrast, the convective dehydration on the bottom of the samples in the wire-to-plate configuration is limited. Moreover, blockage of the airflow with the plate increases the vapor pressure around the samples. In other words, the moist air cannot pass through easily and recirculates on the plate (Figure 3). Each time that the airflow recirculates, it entrains more moisture from the samples, whereas moist air removal is limited. Hence, vapor pressure around the samples increases and results in a lower drying rate (Table 2).

It is noteworthy that the higher the airflow turbulence level, the better the convective dehydration [31,32]. That is why the plate collector performs better than the mesh in lower loading densities (Figure 2c and d). There are fewer samples on the collectors in lower loading densities, so lower humidity will be accumulated in the recirculating air. In this situation, the airflow around the samples on the plate has a higher turbulence level than the samples on the mesh for almost the same vapor pressure, which results in a better drying rate. These phenomena are probably the reason for a better drying performance of the plate collector in very low loading density.

Figure 2c shows when a plate is employed as a collector, drying time is highly affected by the loading density. These results prove that the conventional plate collector used so far in research lab-scale setups has a limited drying capacity which is against the first principle of scalability, i.e., replication.

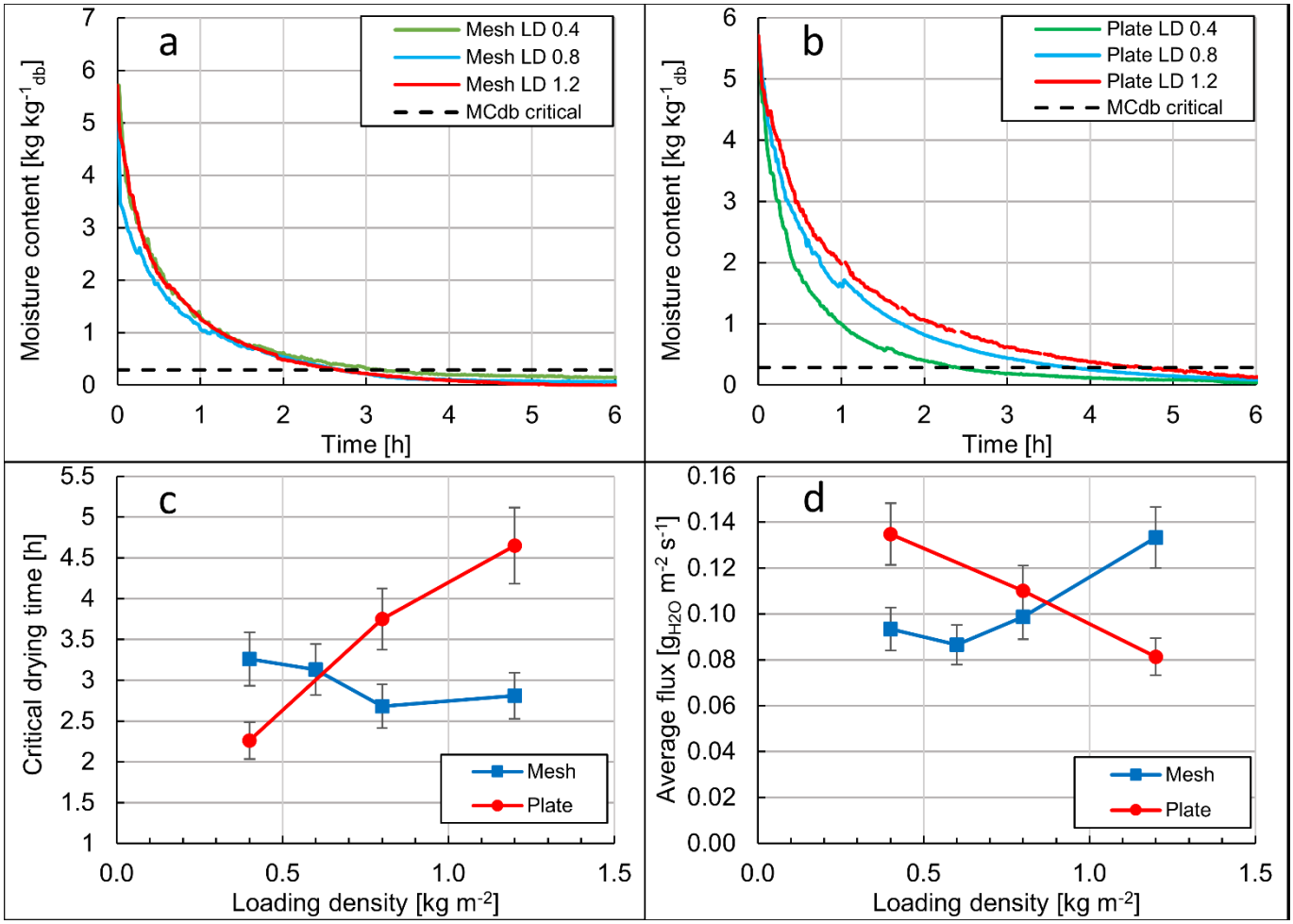

Figure 2 Drying kinetics parameters for optimized wire-to-mesh vs. wire-to-plate in different loading densities; a) dry basis moisture content for optimized mesh collector, b) dry basis moisture content for plate collector, c) critical drying time, d)average drying flux.

Table 2 Average drying rate* and specific drying rate* of the optimized-scalable mesh collector vs. plate collector in different loading densities.

	Mesh LD 0.4	**Mesh LD 0.8**	**Mesh LD 1.2**	**Plate 0.4**	**LD**	**Plate 0.8**	**LD**	**Plate LD 1.2**
Drying rate [g h^{-1}]	6.7	12.8	22.9	9.6		14.7		14.0
Specific drying Rate (SDR) [g_{H2O} kg^{-1}_{db} s^{-1}]	0.36	0.35	0.41	0.52		0.40		0.25

* From beginning of the drying to critical drying time.

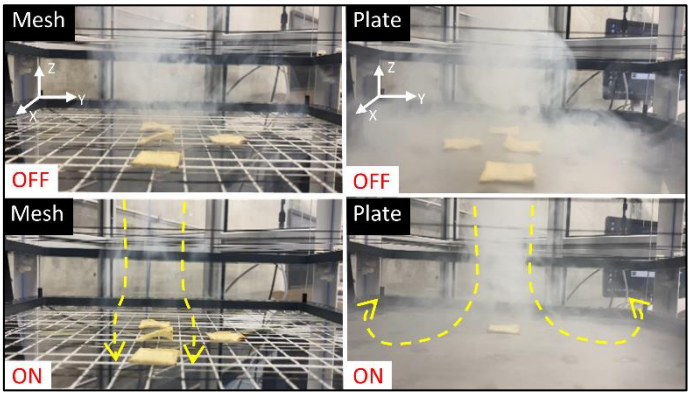

Figure 3 Smoke-flow visualization of the ionic wind for wire-to-mesh and wire-to-plate configurations in EHD ON and OFF modes. Pictures are taken 10 seconds after releasing the smoke with the same smoke intensity.

3.2. Impact of the EHDD configurations on the energy consumption

The energy performance evaluation of the optimized mesh collector and conventional plate collector is presented in this section. The results are shown in Figure 4Figure 2. The energy efficiency of the optimized mesh wire-to-mesh continuously increases with increasing the loading density up to 1.2 kg m^{-2}. In contrast, the drying efficiency of the wire-to-plate configuration does not increase after a loading density of 0.8 kg m^{-2}. Moreover, the results show that by loading a higher amount of fruits, the specific energy consumption (SEC) decreases. Interestingly, the wire-to-plate configuration shows lower SEC in very low loading densities, but its performance deteriorates in higher loading densities. The reason could be attributed to the airflow distribution, and saturation of the moist air above the samples explained in the previous section. Note that reaching an energy efficiency above 100% is meaningful as based on the definition of the energy efficiency described in 2.2.2, natural drying has infinite efficiency. Overall, the results verify that the scalability, in terms of the drying capacity of the optimized mesh collector, is higher than the plate collector from an energy consumption point of view.

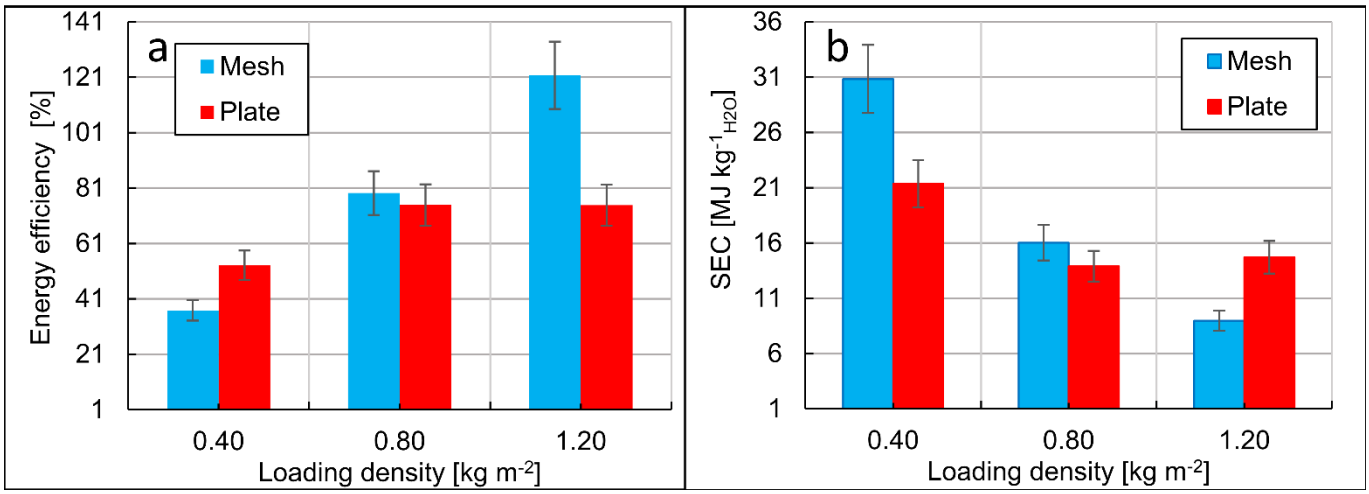

Figure 4 a) Energy efficiency of the optimized mesh collector vs. plate collector in different loading densities, b) specific energy consumption (SEC) of the optimized mesh collector vs. plate collector in different loading densities.

3.3. Performance characterization of the optimized wire-to-mesh configuration

3.3.1. Volumetric flow rate, specific energy consumption, and critical drying time in different discharge power

The performance of the novel optimized wire-to-mesh configuration for different discharge powers is characterized in this section. The results are shown in Figure 5. The critical drying time for the control test (i.e., zero voltage, natural convection) was about 7h and 40 min. The drying time decreases to 3h and 40 min when EHD with the lowest possible power, or so-called inception power, is applied. The EHD inception power is the minimum power by which airflow is generated. This power was about 1 W in our setup. By starting the EHD process, the drying time became a negative linear function of the power (Figure 5). Increasing power from 1W to 11.2W improved the drying time by 33%.

The volumetric flow rate and specific energy consumption (SEC) are nonlinear functions of the discharge power. The same relation between power and flow rate can be seen in axial flow fans [33]. The volumetric flow rate produced by our lab-scale setup is below

200 [$m^3\ h^{-1}$]. For this range of flow rates, computer fans are the most energy-efficient type of fans. Examples of these fans are listed in Table 3 for comparison purposes. Although our configuration's primary purpose was not to deliver the highest volumetric flow, producing airflow by this configuration was more efficient than the most energy-efficient type of fans, as shown in Table 3.

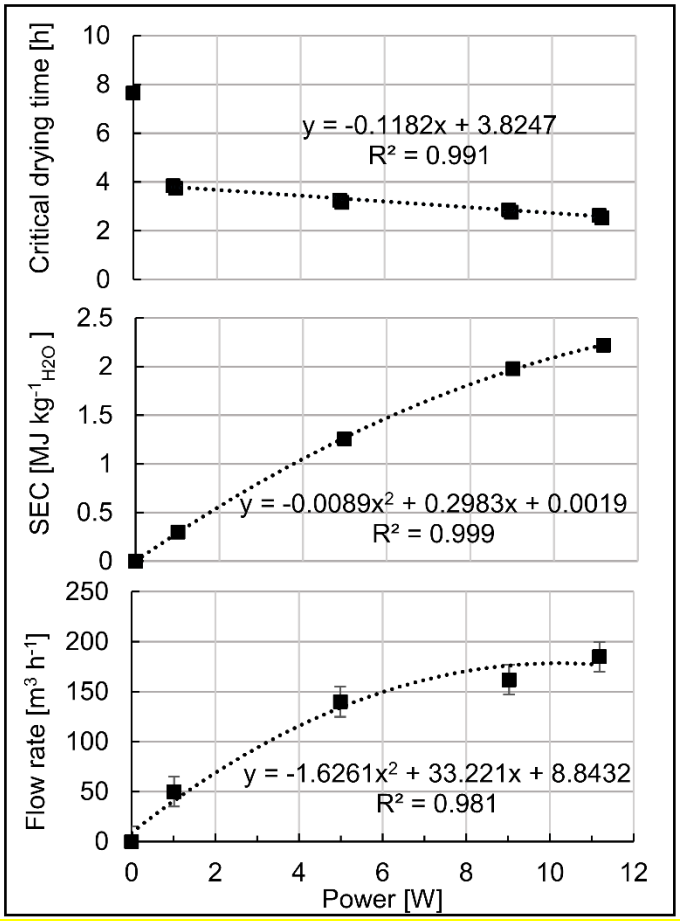

Figure 5 Performance characterization of the optimized wire-to-mesh configuration; Volumetric flow rate, specific energy consumption (SEC), and critical drying time in different discharge power

Table 3 Examples of energy-efficient computer fans

Model, Company, Country	Input power [w]	Volumetric flow rate [$m^3\ h^{-1}$]
OD9238-48HBIP69K, Orion Fans, U.S.	12	170
Kaze Flex 120 Case Fan, Scythe EU GmbH, Germany	5.5	151
CL-F121-PL12GM-A, Thermaltake Technology Co., Ltd., Taiwan	2.8	120

3.3.2. The surface temperature of apple slices during EHD drying

The surface temperature of the drying materials is monitored by the infrared thermography method as described in 2.1.5. The graph in Figure 6 indicates that by starting the drying process, the average surface temperature of the drying materials drops to the wet-bulb temperature (about 15.4 ˚C at RH=50% and $T_{ambient}$=22 ˚C) due to the latent heat of evaporation. Up to the wet-bulb temperature, Figure 6 represents the temperature evolution of the maximum and constant drying rate stage. Continuing the drying process reduces the water content of the material, which in turn decreases the evaporation rate (i.e., falling drying rate stage). This period is driven by the low water transport and increasing the surface temperature to the air temperature until the samples are dried and the evaporation process stops. Therefore, at the end of the drying process, the surface temperature of the dried materials is very close to the room (ambient) temperature. The infrared thermography pictures prove that the optimized wire-to-mesh configuration can dry large amounts of food products in a uniform way.

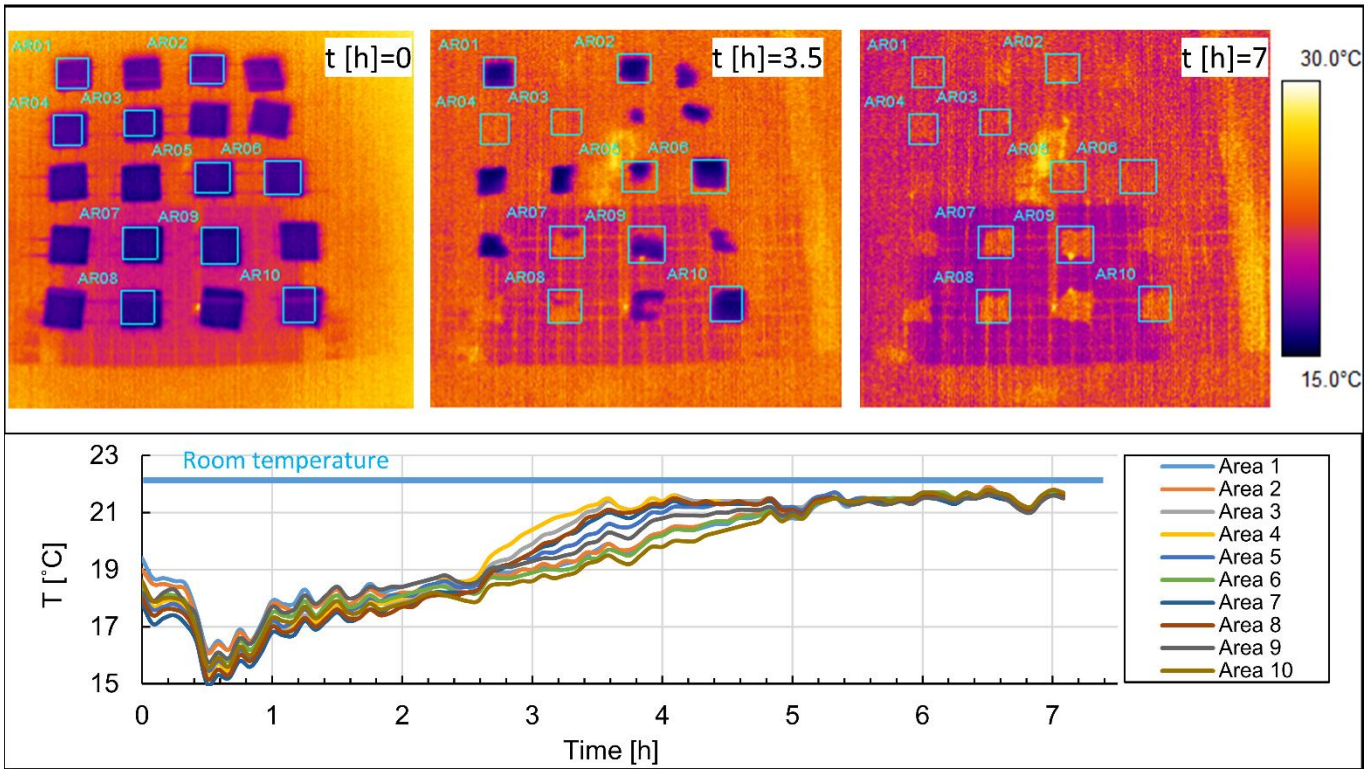

Figure 6 Surface temperature of the drying samples (Mesh LD 0.4) via infrared thermography at the beginning (t [h]=0), middle (t [h]=3.5), and end of the drying time((t [h]=7), together with the average temperature of the ten selected samples vs. time.

4. Discussion

In previous sections, we analyzed the performance of the conventional EHDD configuration (wire-to-mesh) and the novel EHDD configuration (wire-to-mesh). This study experimentally confirmed the previous multiphysics simulation results on the advantages of using mesh collectors instead of plate collectors; As predicted by [13], we observed that wire-to-mesh shows better scalability in terms of production capacity compared to the conventional wire-to-plate configuration. We also identified that the optimized wire-to-mesh configuration proposed by [16] is more energy efficient. However, the improvement factor was not as high as predicted by their simulation study.

In Figure 7, we gathered the most important performance indices in one spider chart to have an overview of the overall performance of these configurations. In addition, the performance of a hot-air dryer under similar drying conditions is also included in the figure. Although the hot-air dryer dries faster, the EHDD configurations perform significantly better in energy consumption and drying efficiency. It is worth mentioning that the process temperature in hot-air drying was about 70˚C, which is not suitable for heat-sensitive compounds like vitamin C. However, this graph only shows a specific case for each of the drying methods. Note that the overall performance of the hot air dryer depends on airspeed, elevated supply air temperature, and humidity of the environment. The performance of the EHD dryer depends on the applied voltage, the ambient supply air temperature, and the humidity of the environment.

Regarding the conventional and novel EHDD configurations, the optimized mesh collector (wire-to-mesh) shows higher scalability than the plate collector (wire-to-plate). Therefore, we recommend using this novel EHDD configuration (wire-to-mesh) for industrialization purposes. Moreover, previous studies on emitters showed a better performance in needle emitters compared to the wire emitter [20,21]. However, using needles as the emitter is not as straightforward as wire for upscaling from the manufacturing point of view. The scalability of discharge electrodes using different types of emitters needs further investigation.

There are still some practical hurdles for industrial implementation of EHDD that should be tackled:

- Some industries are interested in continuous drying processes instead of batch drying processes. An example is the application of EHD on a moving belt. This requires more complex designs and corresponding experiments.
- Working in a high voltage environment requires safety considerations in the design and new safety protocols, training, and maintenance for the industry.
- Ozone and nitrous oxide are the byproduct of EHD. Human lungs can be adversely affected by exposure to these gases. Therefore, the safety thresholds of 60-70 ppb of ozone for 8 h [34,35] should be respected in future industrial applications. Of course, ozone can be considered positive for the food industry for specific applications as it disinfects and kills pathogens.

- Most of the EHD drying tests are conducted under atmospheric pressure and room temperature in the air. The functionality of the EHD dryers under different ambient conditions should be identified.

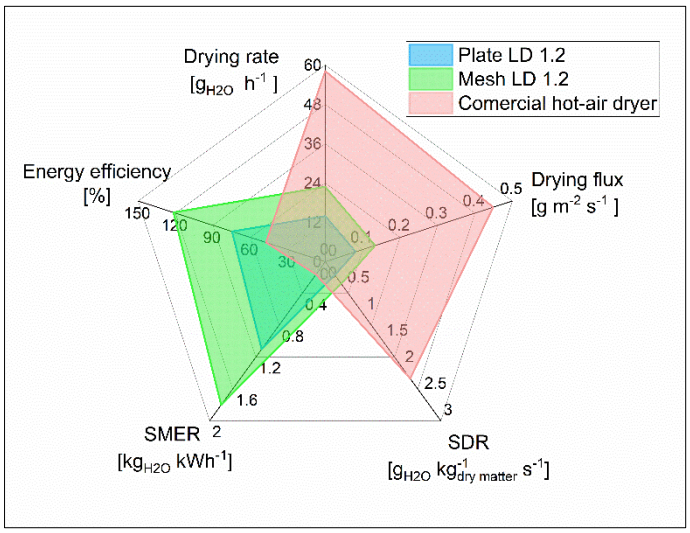

Figure 7 Overall performance of the conventional EHDD configuration (plate collector) and the novel EHDD configuration (optimized mesh collector) compared to a hot-air dryer.

5. Conclusion

The scalability of the conventional EHDD configuration (wire-to-plate) and the novel optimized wire-to-mesh was evaluated in this study. An upscalable experimental setup for non-intrusive measurement was developed. The results showed that the optimized mesh collector keeps its good performance independent from the amount of loaded fruit. This novel configuration is more scalable than the conventional plate collector from drying kinetics and energy consumption perspectives. Employing the optimized mesh collector instead of the plate collector improves the drying rate and energy efficiencies by more than 60%. Moreover, the novel EHDD configuration is 2.6 times more energy-efficient compared to the commercial hot-air dryer. However, the drying rates of the EHDD configurations are lower than the commercial hot-air dryer.

In this regard, the performance of the novel optimized wire-to-mesh configuration in different discharge powers was characterized. The characterization tests revealed that drying time, specific energy consumption, and volumetric flow rate are negative linear, negative hyperbolic, and negative hyperbolic functions of the applied power, respectively. In addition, the infrared thermography pictures proved that the optimized wire-to-mesh configuration could uniformly dry large amounts of food products. Overall, this study verifies that the optimized mesh collector should be considered for upscaling purposes.

6. Acknowledgment

The authors acknowledge the ETH Foundation and the World Food System Center of ETH Zurich for supporting this project.

7. Author contributions

Kamran Iranshah: Conceptualization, Methodology, Investigation, Experimentation, Project administration, Writing-Original draft, Review & Editing. **Daniel Onwude**: Methodology, Review & Editing. **Donato Rubinetti**: Review & Editing. **Alex Martynenko**: Review & Editing. **Thijs Defraeye**: Conceptualization, Methodology, Supervision, Project administration, Review & Editing.

8. REFERENCES

[1] Hasan Masud M, Karim A, Ananno AA, Ahmed A. Sustainable Food Drying Techniques in Developing Countries: Prospects and Challenges. Cham: Springer International Publishing; 2020. https://doi.org/10.1007/978-3-030-42476-3.

[2] UN FAO. How can we feed the world in 2050? FAO WSFS 2019:1–35. http://www.fao.org/fileadmin/templates/wsfs/docs/expert_paper/How_to_Feed_the_World_in_2050.pdf.

[3] Alasalvar C, Salvadó J-S, Ros E. Bioactives and health benefits of nuts and dried fruits. Food Chem 2020;314:126192. https://doi.org/10.1016/j.foodchem.2020.126192.

[4] Motevali A, Minaei S, Banakar A, Ghobadian B, Khoshtaghaza MH. Comparison of energy parameters in various dryers. Energy Convers Manag 2014;87:711–25. https://doi.org/10.1016/j.enconman.2014.07.012.

[5] Defraeye T, Martynenko A. Future perspectives for electrohydrodynamic drying of biomaterials. Dry Technol 2018;36:1–10. https://doi.org/10.1080/07373937.2017.1326130.

[6] Singh A, Orsat V, Raghavan V. A Comprehensive Review on Electrohydrodynamic Drying and High-Voltage Electric Field in the Context of Food and Bioprocessing. Dry Technol 2012;30:1812–20. https://doi.org/10.1080/07373937.2012.708912.

[7] Alemrajabi AA, Rezaee F, Mirhosseini M, Esehaghbeygi A. Comparative evaluation of the effects of electrohydrodynamic, oven, and ambient air on carrot cylindrical slices during drying process. Dry Technol 2012;30:88–96. https://doi.org/10.1080/07373937.2011.608913.

[8] Singh A, Vanga SK, Nair GR, Gariepy Y, Orsat V, Raghavan V. Electrohydrodynamic drying (EHD) of wheat and its effect on wheat protein conformation. LWT - Food Sci Technol 2015;64:750–8. https://doi.org/10.1016/J.LWT.2015.06.051.

[9] Bajgai TR, Raghavan GSV, Hashinaga F, Ngadi MO. Electrohydrodynamic drying - A concise overview. Dry Technol 2006;24:905–10. https://doi.org/10.1080/07373930600734091.

[10] Esehaghbeygi A, Basiry M. Electrohydrodynamic (EHD) drying of tomato slices (Lycopersicon esculentum). J Food Eng 2011;104:628–31. https://doi.org/10.1016/j.jfoodeng.2011.01.032.

[11] Martynenko A, Kudra T. Electrohydrodynamic (EHD) drying of grape pomace. Japan J Food Eng 2016;17:123–9. https://doi.org/10.11301/jsfe.17.123.

[12] Tuan A, Tam T, Ngoc A, Lang V, Chyuan F. Application of EHD-enhanced drying technology : a sustainable approach for Vietnam ' s agricultural product processing in the future. J Viet Env 2014;6:256–63. https://doi.org/10.13141/jve.vol6.no3.pp256-263.

[13] Defraeye T, Martynenko A. Electrohydrodynamic drying of multiple food products: Evaluating the potential of emitter-collector electrode configurations for upscaling. J Food Eng 2019;240:38–42. https://doi.org/10.1016/j.jfoodeng.2018.07.011.

[14] Bondi AB. Characteristics of scalability and their impact on performance. Proc. Second Int. Work. Softw. Perform. - WOSP '00, New York, New York, USA: ACM Press; 2000, p. 195–203. https://doi.org/10.1145/350391.350432.

[15] Putnik G, Sluga A, ElMaraghy H, Teti R, Koren Y, Tolio T, et al. Scalability in manufacturing systems design and operation: State-of-the-art and future developments roadmap. CIRP Ann 2013;62:751–74. https://doi.org/10.1016/j.cirp.2013.05.002.

[16] Iranshahi K, Martynenko A, Defraeye T. Cutting-down the energy consumption of electrohydrodynamic drying by optimizing mesh collector electrode. Energy 2020;208:118168. https://doi.org/10.1016/j.energy.2020.118168.

[17] Mohan VPC, Talukdar P. Experimental studies for convective drying of potato. Heat Transf. Eng., vol. 35, Taylor & Francis Group; 2014, p. 1288–97. https://doi.org/10.1080/01457632.2013.876844.

[18] Zlatanović I, Komatina M, Antonijević D. Low-temperature convective drying of apple cubes. Appl Therm Eng 2013;53:114–23. https://doi.org/10.1016/j.applthermaleng.2013.01.012.

[19] Horwitz W, Chichilo P, Reynolds H. Official methods of analysis of the Association of Official Analytical Chemists. Washington - D.C: AOAC; 1970.

[20] Martynenko A, Iranshahi K, Defraeye T. Plate versus mesh collecting electrode for electrohydrodynamic (EHD) drying. Https://DoiOrg/101080/073739320211962338 2021. https://doi.org/10.1080/07373937.2021.1962338.

[21] Bashkir I, Martynenko A. Optimization of multiple-emitter discharge electrode for electrohydrodynamic (EHD) drying. J Food Eng 2021;305:110611. https://doi.org/10.1016/j.jfoodeng.2021.110611.

[22] Elmizadeh A, Shahedi M, Hamdami N. Comparison of electrohydrodynamic and hot-air drying of the quince slices. Innov Food Sci Emerg Technol 2017;43:130–5. https://doi.org/10.1016/j.ifset.2017.07.030.

[23] R Core Team. R: A Language and Environment for Statistical Computing 2021.

[24] ISO 18434-1:2008. Condition monitoring and diagnostics of machines — Thermography — Part 1: General procedures. ICS 2008:24. https://www.iso.org/standard/41648.html (accessed January 29, 2022).

[25] Defraeye T, Verboven P. Convective drying of fruit: Role and impact of moisture transport properties in modelling. J Food Eng 2017;193:95–107. https://doi.org/10.1016/j.jfoodeng.2016.08.013.

[26] Iranshahi K, Onwude DI, Martynenko A, Defraeye T. Dehydration mechanisms in electrohydrodynamic drying of plant-based foods. Food Bioprod Process 2022;131:202–16. https://doi.org/10.1016/J.FBP.2021.11.009.

[27] Leon MA, Kumar S, Bhattacharya SC. A comprehensive procedure for performance evaluation of solar food dryers. Renew Sustain Energy Rev 2002;6:367–93. https://doi.org/10.1016/S1364-0321(02)00005-9.

[28] Menon A, Stojceska V, Tassou SA. A systematic review on the recent advances of the energy efficiency improvements in non-conventional food drying technologies. Trends Food Sci Technol 2020;100:67–76. https://doi.org/10.1016/J.TIFS.2020.03.014.

[29] Mujumdar AS. Handbook of Industrial Drying. CRC Press; 2014. https://doi.org/10.1201/b17208.

[30] Kudra T. Energy Aspects in Drying. Dry Technol 2004;22:917–32. https://doi.org/10.1081/DRT-120038572.

[31] Carrera-Escobedo J, Guzman-Valdivia C, Ortiz-Rivera A, Garcia-Ruiz M, Cruz-Dominguez O. Quantitative assesment of the improvement of the drying process by increasing the turbulence level. Therm Sci 2019;23:953–63. https://doi.org/10.2298/TSCI170509189C.

[32] Martynenko A, Astatkie T, Defraeye T. The role of convection in electrohydrodynamic drying. J Food Eng 2020;271:109777. https://doi.org/10.1016/j.jfoodeng.2019.109777.

[33] Bleier FP. Fan Handbook: selection, application, and design. McGraw-Hill; 2018.

[34] EPA U. NAAQS Table | US EPA 2019. https://www.epa.gov/criteria-air-pollutants/naaqs-table (accessed January 26, 2022).

[35] European Commission. Standards - Air Quality - Environment - European Commission. Eur Comm 2017. https://ec.europa.eu/environment/air/quality/standards.htm (accessed January 26, 2022).